NeuroImage 92 (2014) 56–68

Contents lists available at ScienceDirect

NeuroImage

journal homepage: www.elsevier.com/locate/ynimg

A conceptual model for CO_2-induced redistribution of cerebral blood flow with experimental confirmation using BOLD MRI

O. Sobczyk [a], A. Battisti-Charbonney [b], J. Fierstra [c], D.M. Mandell [b], J. Poublanc [b], A.P. Crawley [b], D.J. Mikulis [b], J. Duffin [d,e,*], J.A. Fisher [a,d,e]

[a] Institute of Medical Sciences, University of Toronto, Toronto, Canada
[b] Joint Department of Medical Imaging and the Functional Neuroimaging Laboratory, University Health Network, Toronto, Canada
[c] Department of Neurosurgery, University Hospital Zurich, Zurich, Switzerland
[d] Department of Anaesthesia and Pain Management University Health Network, University of Toronto, Canada
[e] Department of Physiology, University of Toronto, Canada

ARTICLE INFO

Article history:
Accepted 27 January 2014
Available online 5 February 2014

Keywords:
Cerebrovascular reactivity
Carbon dioxide
Steal
Reverse steal
Humans

ABSTRACT

Cerebrovascular reactivity (CVR) is the change in cerebral blood flow (CBF) in response to a change in a vasoactive stimulus. Paradoxical reductions in CBF in response to vasodilatory stimulation ('steal') are associated with vascular pathology. However, a pathophysiological interpretation of 'steal' requires a comprehensive conceptual model linking pathology and changes in blood flow. Herein, we extend a simple model explaining steal published in the late 1960s by incorporating concepts of CBF regulation from more recent studies to generate a comprehensive dynamic model. The main elements of the model are: (a) the relationship between changes in CBF and the arterial partial pressure of carbon dioxide ($PaCO_2$) in healthy vascular regions is sigmoidal; (b) vascular regions vasodilate to compensate for decreased perfusion pressure, leading to (c) an encroachment on vasodilatory reserve and, reduced CVR; (d) a vasodilatory stimulus may increase CBF capacity above the flow capacity of major cerebral blood vessels; and (e) this limitation induces competitive intra-cerebral redistribution of flow from territories with low vasodilatory reserve to those with high reserve. We used CVR measurements generated by applying precise, computer-controlled changes in $PaCO_2$ as the vasoactive stimulus, and measured blood oxygen level dependent (BOLD) MRI signals as high resolution surrogates of CBF to test predictions derived from this model. Subjects were 16 healthy adults and 16 patients with known cerebral steno-occlusive diseases. We observed regional sigmoidal $PaCO_2$–BOLD response curves with a range of slopes; graded changes in $PaCO_2$ resulted in redistributions of BOLD signal consistent with the known underlying vascular pathology and predictions of the model. We conclude that this model can be applied to provide a hemodynamic interpretation to BOLD signal changes in response to hypercapnia, and thereby aid in relating CVR maps to pathophysiological conditions.

© 2014 Elsevier Inc. All rights reserved.

Introduction

Dilation of cerebral vessels can result, paradoxically, in reductions of blood flow in certain regions. This phenomenon is associated with an enhanced risk of stroke (Kleiser and Widder, 1992; Markus and Cullinane, 2001; Molina et al., 1999; Ogasawara et al., 2002; Sasoh et al., 2003; Webster et al., 1995; Yonas et al., 1993) and dementia (Marshall and Lazar, 2011; Silvestrini et al., 2011; Zhao et al., 2009). What is not well understood is how these two observations are linked. If we could better elucidate the mechanism of vasodilator-induced redistributions of blood flow in the brain, we may better understand the pathophysiology of the diseases with which they are associated.

Herein, we begin with a conceptual model described in 1968 by Brawley (1968) and Symon (1968) and apply physiologic insights derived from some more recent pivotal studies to transform it into a dynamic model relating vasodilator-induced changes in regional cerebral blood flow (rCBF) to underlying vascular pathology (Appendix A). We then test the predictions of our model by applying precise automated changes in the partial pressure of CO_2 in arterial blood ($PaCO_2$), and observing the response of Blood Oxygen Level Dependent (BOLD) MRI signals as high resolution surrogates of rCBF.

A model of distribution of rCBF in response to cerebral vascular stimulation

The major vessels of the cerebral circulation generate about 30% of the total cerebrovascular resistance to flow, a greater resistance than similarly sized vessels supplying any other organ (Faraci and Heistad, 1990). Moreover, the major intracranial branches, far from being simple conduits, can add another 20% of flow resistance upstream from the pial

* Corresponding author at: Department of Physiology, Medical Sciences Building, 1 King's College Circle, University of Toronto, Toronto, Ontario M5S 1A8, Canada. Fax: +1 416 597 1330.
E-mail address: j.duffin@utoronto.ca (J. Duffin).

1053-8119/$ – see front matter © 2014 Elsevier Inc. All rights reserved.
http://dx.doi.org/10.1016/j.neuroimage.2014.01.051

vessels (Iadecola and Nedergaard, 2007). The net perfusion pressure for any regional vascular territory of the brain is, therefore, the systemic blood pressure minus any reductions in pressure due to flow resistance in the major extra-cranial vessels and vessels arising from the Circle of Willis.

The flow resistances in cerebral vascular territories can respond to upstream changes in vascular tone, or to the presence of fixed stenotic lesions, in the direction of maintaining rCBF (cerebral autoregulation) (Hill et al., 2006; Lucas et al., 2010) (Fig. 1). However, such compensatory reductions in vascular tone have physical limits. The difference between baseline vessel tone and this limit constitutes a *vasodilatory reserve*. Note that although we develop the model on the basis of regional vascular stenosis where "autoregulatory reserve" is appropriate, we prefer the term 'vasodilatory reserve' as it is more general and can also be applied to vessels that are plegic due to, for example, drugs, developmental vascular abnormalities, vascular disease, or trauma. Because of the high extra-cerebral arterial resistance and robust downstream vasodilatory reserve, the overall CBF capacity may exceed its potential supply (Brawley, 1968; Faraci and Heistad, 1990). Thus, a large vasodilatory stimulus would set up vascular beds, perfused in parallel by a common feed vessel, in competition for a limited flow of blood. Vessels with the greater vasodilatory reserve will increase their flow at the expense of those with the lesser reserve, a phenomenon termed 'steal' (Faraci and Heistad, 1990).

Fig. 2 represents a more detailed and extended model incorporating the physiologic principles derived from more recent studies (Appendix A). Vascular territories with full vasodilatory reserve respond to a range of $PaCO_2$ with a large amplitude sigmoidal pattern of rCBF (Fig. 2 solid line). The flow through a branch with reduced vasodilatory reserve, if stimulated in isolation, would also have a sigmoidal pattern of response to the stimulus, but its resting tone would be closer to its maximal dilated state, and its response to a range of $PaCO_2$ would be dampened, exhibiting a smaller range of response (from maximal constriction to maximum dilation), and gain (change of tone for a change of stimulus) (Appendix A).

But if the stimulus is applied to the entire vascular bed, the distribution of blood flow depends on the interaction of 3 conditions: 1) the resistance of the feed vessel, 2) the magnitude of the stimulus and 3) the relative regional vasodilatory reserve. Some vessels with reduced vascular reserve (blue dashed line) may be capable of reducing their resistance sufficiently to increase their blood flow at small increases in $PaCO_2$; but with further increases in $PaCO_2$ their share of the blood flow declines as it is redistributed to the vascular beds with the more robust vasodilation. Similarly, small decreases in $PaCO_2$ may reduce flow to both healthy and compromised vessels, but this enhanced model predicts that larger reductions in $PaCO_2$ will cause a redistribution of blood flow *in favor* of the compromised vessels, i.e., reverse steal.

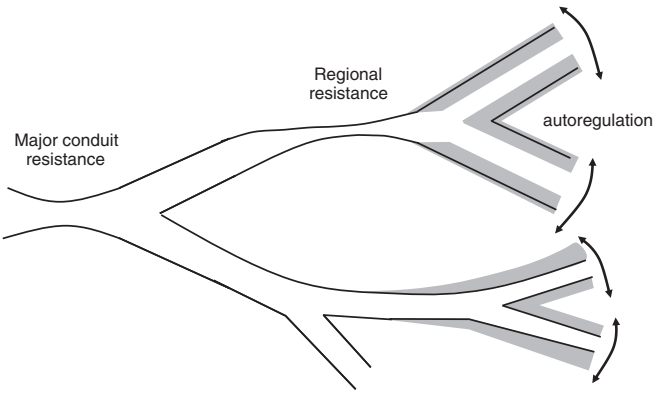

Fig. 1. A schematic representing a brain vascular territory with a partially-stenosed vessel branch and a healthy branch in parallel supplied by a major conduit vessel with restricted flow reserve. The vasodilatory reserves of the downstream vessels are shaded. In the upper vessel, autoregulation has encroached on the vasodilatory reserve. A vasodilatory stimulus such as an increase in $PaCO_2$ will stimulate all vessels to dilate, but the increase in flow in the vessel with preserved vasodilatory reserve will reduce the perfusion pressure, and thereby the flow distal to the regional resistance.

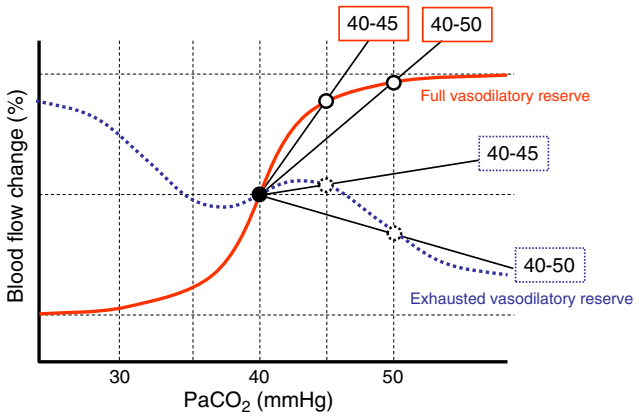

Fig. 2. Predicted blood flow responses to $PaCO_2$ for an enhanced version of the model shown in Fig. 1, as developed in Appendix A. The solid red line depicts the sigmoidal response of a vascular bed with normal vasodilatory reserve. The dotted blue line depicts the flow in a vessel with reduced vasodilatory reserve. In isolation it would have a flattened sigmoidal shape compared to the red curve. However, in this model it is coupled in parallel with a vessel with normal vascular reserve, and the supply capacity of their feed vessel is less than the combined flow capacity of two vascular beds. Testable predictions of the model are that cerebrovascular reactivity (CVR), measured as Δ%BOLD signal/$\Delta PaCO_2$ will be greater for smaller changes of $PaCO_2$ (40–45 mm Hg) than greater changes (40–50 mm Hg). Note that the model predicts that a vascular territory downstream from a hemodynamically significant stenosis may have a positive CVR when the $PaCO_2$ change is in a range where some vasodilatory reserve is preserved (e.g., in this figure, between 40 and 45 mm Hg). However, with a greater stimulus, these vessels reach their vasodilatory limit and the continued vasodilatory response in other regions will induce steal (downsloping line). A family of lines can be imagined undergoing incremental intermediate changes between the red and blue lines, and beyond, representing various CVR values depending on the magnitude, and direction, of the stimulus.

The aim of this study was to test the following fundamental aspects of the enhanced model: (1) the relationship between $PaCO_2$ and rCBF is sigmoidal; and (2) the net distribution of blood flow between vascular territories reflects (a) their respective regional vasodilatory reserve and (b) the magnitude of the stimulus. We tested these aspects of the model in healthy subjects and those with known cerebral vascular steno-occlusive disease by administering a range of $PaCO_2$ between hypocapnia and hypercapnia, and monitoring BOLD MRI signals.

Methods

Review of literature for historical data to enhance the model

The brain vascular reactivity literature contains many combinations of stimulation methods, stimulation patterns, and surrogates of CBF. Because this heterogeneity made it impossible to select search terms that would result in a manageable number of relevant articles, we manually searched for studies in which: vasoconstrictor and vasodilator stimuli were applied (e.g., hyperventilation and rebreathing); subjects had regions with reduced vasodilatory reserve (e.g., due to vascular stenosis or hypotension); and rCBF was reported with adequate temporal and spatial resolution. Data from these studies were used to enhance various aspects of the basic model (Appendix A).

Human subjects

These studies conformed to the standards set by the latest revision of the Declaration of Helsinki. All studies were approved by the Research Ethics Board of the University Health Network and all subjects were competent and gave written informed consent.

Patients were referred to our medical imaging department by neurology or neurosurgery consultants for investigations of transient neurological symptoms suggestive of hemodynamic compromise. We recruited subjects with angiographically apparent large vessel cervical or cerebral artery steno-occlusive disease. Our healthy cohort was recruited by advertisement and word of mouth. The healthy subjects were of any age and either sex, and did not smoke or take any prescribed medication. All subjects were asked to refrain from caffeine, tobacco, or heavy exercise on the day of the examination. Their characteristics are detailed in Table 1.

Experimental protocol

Each subject participated in a protocol consisting of a reduction in $P_{ET}CO_2$ to 30 mm Hg for 30 s, induced by voluntary hyperventilation, followed by a linear progressive rise ('ramp') of $P_{ET}CO_2$ reaching 55 mm Hg over 4 min, and a return to baseline (see Fig. 5). Throughout, the end-tidal partial pressure of O_2 ($P_{ET}O_2$) was held constant at 100 mm Hg. We compared the changes in BOLD signal in response to two levels of change in $P_{ET}CO_2$, of two overlapping ranges, 40–45 mm Hg and 40–50 mm Hg, in the same subject.

Apparatus

Subjects were fitted with a face mask, and connected to a sequential gas delivery breathing circuit (Slessarev et al., 2007). The patterns of $P_{ET}CO_2$ and $P_{ET}O_2$ were programmed into the automated gas blender, which directed mixtures of O_2, CO_2, and N_2 into the breathing circuit according to prospective targeting algorithms (Slessarev et al., 2007). Tidal gas was sampled and analyzed for $P_{ET}CO_2$ and $P_{ET}O_2$ (RespirAct™, Thornhill Research Inc., Toronto, Canada) and recorded at 20 Hz. Our laboratory (Fierstra et al., 2011; Ito et al., 2008) and others (Brogan et al., 2004; Willie and Ainslie, 2011) have shown that end-inspiratory rebreathing, (also employed by the RespirAct™), results in $P_{ET}CO_2$ being equal to $PaCO_2$ within the range of measurement error. Therefore, in this paper, we use $PaCO_2$ when referring to the independent variable affecting brain blood flow, and $P_{ET}CO_2$ when referring to actual measurements made by the RespirAct™.

Magnetic resonance imaging was performed with a 3.0-Tesla HDx scanner using an 8-channel phased-array receiver coil (Signa; GE Healthcare, Milwaukee, Wisconsin) and consisted of BOLD acquisitions with echo planar imaging (EPI) gradient echo (TR/TE = 2000/30 ms, 3.75 × 3.75 × 5 mm voxels, field of view 24 × 24 cm, 30 slices, slice thickness 5 mm, matrix size 64 × 64, number of frames = 254, flip angle (FA) = 85°). The acquired MRI and $P_{ET}CO_2$ data were analyzed using AFNI software (National Institutes of Health, Bethesda, Maryland; http://afni.nimh.nih.gov/afni; (Cox, 1996)). To synchronize $P_{ET}CO_2$ and BOLD signal data, $P_{ET}CO_2$ data were time-shifted to the point of maximum correlation with the BOLD signal averaged over the whole brain. BOLD signal drift correction was made assuming a linear drift over time between the initial and final baselines.

A regression coefficient between $P_{ET}CO_2$ and the BOLD signal was calculated for each voxel. Fig. 3 shows regression coefficient maps for three subjects whose CVR maps are used in later figures, and illustrates the effects of thresholding on the CVR maps. CVR maps in the Results section are shown thresholded at 0.25, where all voxels with a regression coefficient between −0.25 and +0.25 were arbitrarily eliminated

Table 1
Characteristics of patients and healthy volunteers.

Subject	Sex	Age	Condition	Resting $P_{ET}CO_2$ (mm Hg)
1	F	18	Bilateral moyamoya post right EC–IC bypass	37
2	F	28	Moyamoya	28
3	M	24	Steno-occlusive	34
4	F	47	Bilateral moyamoya with RICH	32
5	M	18	Bilateral moyamoya	35
6	F	66	Steno-occlusive	40
7	F	32	Bilateral moyamoya and bilateral ICA occlusion	36
8	F	30	Bilateral ICA occlusion with enlarged EC vessels	35
9	F	36	bilateral moyamoya	37
10	F	41	R moyamoya with bilateral ICA occlusion	35
11	F	21	Moyamoya	34
12	F	63	Bilateral MCA stenosis	35
13	M	18	Bilateral moyamoya	40
14	F	19	Moyamoya	38
15	F	13	Vasculitis ACTA2 mutation	35
16	F	23	Moyamoya	37
17	M	49	Healthy	41
18	M	59	Healthy	36
19	F	33	Healthy	32
20	M	22	Healthy	38
21	M	45	Healthy	33
22	M	63	Healthy	40
23	M	73	Healthy	40
24	M	35	Healthy	37
25	F	28	Healthy	30
26	M	41	Healthy	35
27	M	46	Healthy	40
28	M	33	Healthy	39
29	M	25	Healthy	41
30	M	34	Healthy	40
31	M	41	Healthy	35
32	M	27	Healthy	41

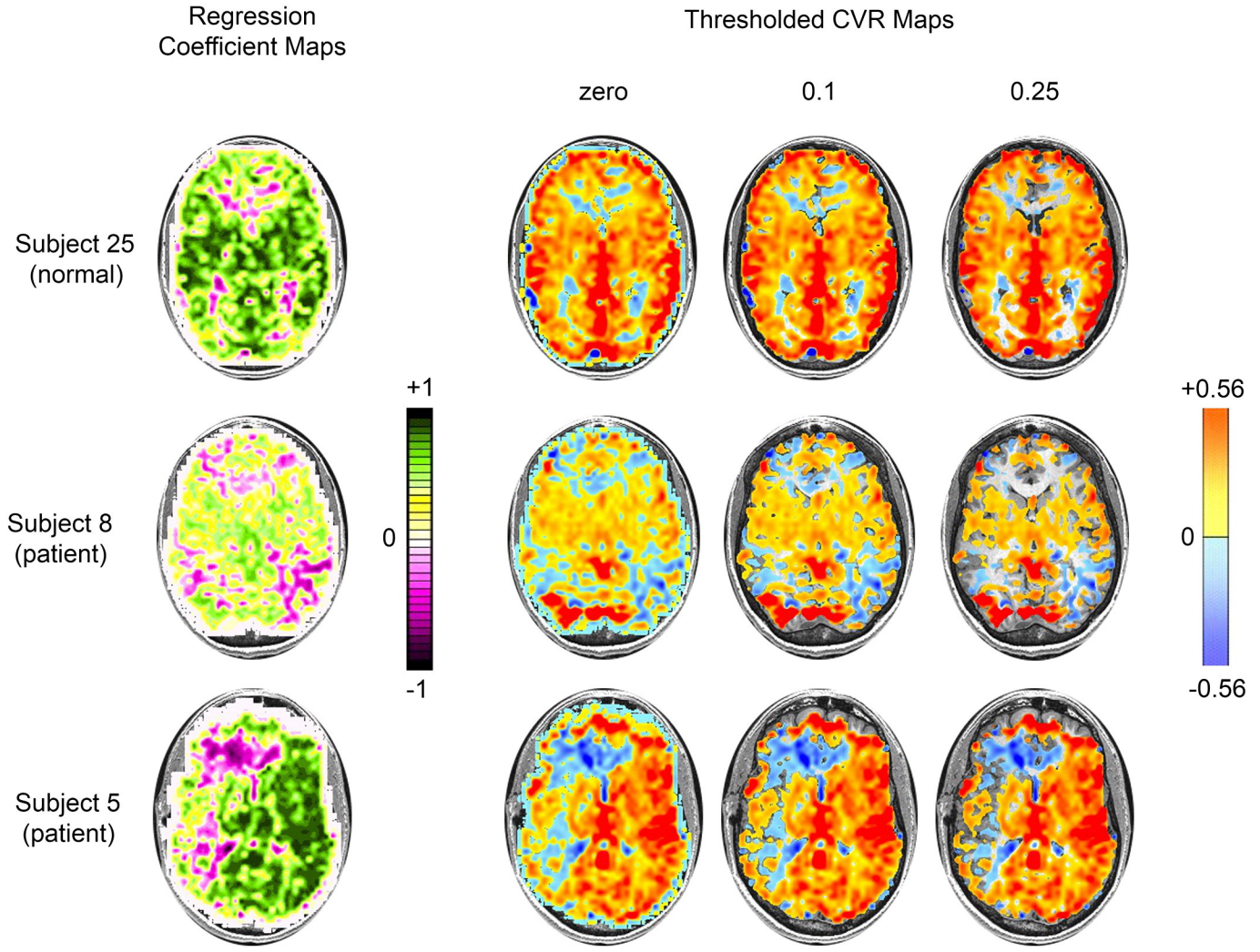

Fig. 3. Regression coefficient maps and corresponding CVR maps (for subjects 25, 8 and 5 found in the Results section). The CVR maps (% BOLD change/mm Hg $P_{ET}CO_2$) were thresholded (see text) according to their corresponding regression coefficient values at zero, 0.1 and 0.25. The maps are colored according to the scales shown.

as "noise". This threshold was chosen to provide the best compromise between sensitivity and specificity. When examining a large number of pathological scans this threshold eliminates voxels with little information (such as the skull borders) and leaves sufficient areas uncolored to allow anatomical orientation of the CVR maps (e.g. Spano et al., 2013). A linear, least-squares fitting of the BOLD signal data series to the $P_{ET}CO_2$ data series was then performed voxel-by-voxel. The slope of the relation between the BOLD signal and the $P_{ET}CO_2$ was color-coded to a spectrum of colors corresponding to the direction (positive or negative) and the magnitude of the correlation.

BOLD images were then volume registered and slice-time corrected, and co-registered to an axial 3-D T1-weighted Inversion-Recovery prepared Fast Spoiled Gradient-Echo (IR-FSPGR) volume (TI/TR/TE = 450/8/3 ms, voxel size 0.86 × 0.86 × 1.0 mm, matrix size 256 × 256, field of view 22 × 22 cm, slice thickness = 1 mm, FA = 15°) that was acquired at the same time (Saad et al., 2009). This method has been described in greater detail elsewhere (Fierstra et al., 2010). All images were normalized by mapping them into the same number of voxels enabling the representation of the fractional frequency of CVR values by constructing frequency distribution histograms (FDHs) using all CVR data except zero values.

Statistical analysis

We examined the effect on changes in BOLD signal in the 40–45 mm Hg and 40–50 mm Hg ranges of $P_{ET}CO_2$ in both our healthy, and patient, cohorts. A two-way analysis of variance with factors CO_2 range (40–45 vs. 40–50 mm Hg) and subject group (patient vs. healthy) was used to compare the effect of stimulus range. If differences were found, post hoc Bonferroni all-pair-wise tests were used to determine which groups differed significantly from one another.

Results

The effect of stimulus strength on CVR maps

Fig. 4A illustrates typical CVR results in a healthy individual (subject 25) for $P_{ET}CO_2$ ranges 40–45 mm Hg and 40–50 mm Hg, and Fig. 4B illustrates typical CVR results in a patient (subject 8) with bilateral internal carotid artery (ICA) occlusion for $P_{ET}CO_2$ ranges 40–45 mm Hg and 40–50 mm Hg. The frequency distribution of CVR with each stimulus shown in Figs. 4A, B can be explained with reference to the model as depicted in Fig. 2. Note that with the smaller stimulus there is a wider

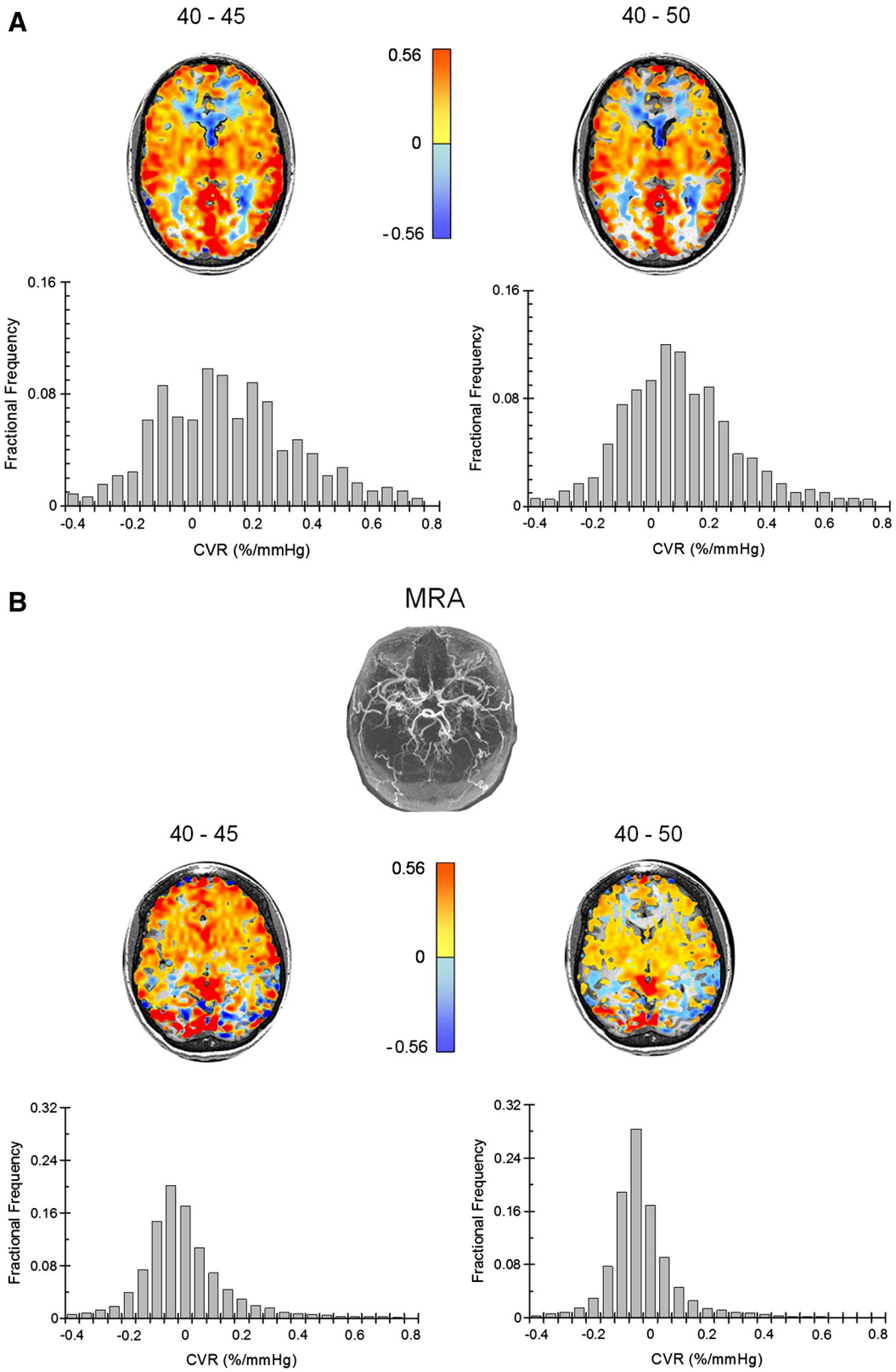

Fig. 4. A) CVR maps obtained from a healthy control subject 25 at two $P_{ET}CO_2$ ranges (40–45 and 40–50 mm Hg). Top: CVR maps for an axial slice showing the spatial distribution of CVR values colored according to the scale shown. The scale is in % BOLD change/mm Hg $P_{ET}CO_2$ change. Bottom: Fractional frequency distribution histograms of the CVR values for the whole brain. B) CVR maps obtained from subject 8 with bilateral internal carotid artery occlusion at two $P_{ET}CO_2$ ranges (40–45 and 40–50 mm Hg). Top: Magnetic resonance angiography (MRA). Middle: CVR maps for an axial slice showing the spatial distribution of CVR values colored according to the scale shown. The scale is in % BOLD change/mm Hg $P_{ET}CO_2$ change. Bottom: Fractional frequency distribution histograms of the CVR values for the whole brain.

range of positive and negative voxels. The reduced number of positive voxels with the greater stimulus is a result of a reduction in the number of voxels which can retain a positive response (e.g. 28% with 40–50 mm Hg vs. 45% with 40–45 mm Hg in the patient frequency distributions). There would be a complementary effect on the negative voxels, reducing their range and increasing their number (e.g. from 20% to 30% in the patient frequency distributions). The smaller range of negative voxels with the greater stimulus also results from the peculiar method of calculating CVR: With additional linear increases in the stimulus from $P_{ET}CO_2$ of 45 mm Hg to 50 mm Hg (in the denominator), the increases in flow to the voxels (i.e., BOLD signal) represented by the red line, are progressively reduced. Thus the wider distribution of the voxels with the lower stimulus results in greater average of both positive (e.g. 0.13 vs. 0.08%/mm Hg for the patient frequency distributions) and negative (e.g. 0.09 vs. 0.03%/mm Hg for the patient frequency distributions) CVR values. Note that despite the greater range of negative voxel values, the total number of negative voxels is similar with the 45–50 mm Hg and the 40–50 mm Hg stimuli (e.g. 20% vs. 30%, respectively for the patient frequency distributions). These patterns are typical of those in the healthy and patient cohorts presented in Table 2.

The mean (SD) CVR for all subjects resulting from the different stimulus ranges is presented in Table 2. The model (Fig. 2) indicates that the interaction of the various vascular beds alters the sigmoidal shape of the responses to hypercapnia. In an attempt to test whether an objective measure would differentiate between maps obtained under the various conditions, we compared the frequency distributions of the CVRs (Fig. 4) by calculating the descriptive characteristics of the distributions such as kurtosis (the degree of scatter of normally distributed data around the mean) and skewness (the symmetry of the distribution of the data around the mean). Neither of these measures proved to be significant factors, but for patients the mean of both the + ve and − ve CVR values was greater, and less, respectively, at the lower stimulus range (*P = 0.04 and †P = 0.03 respectively). A similar pattern was found for the healthy volunteers (§P = 0.008 and #P < 0.001 for Mean + ve and Mean − ve respectively). These findings are illustrated and discussed in reference to the example cases in Fig. 4. Of note is that the % − ve (i.e., proportion of voxels with steal) differed between patients and healthy subjects, but was only statistically significant (¶P = 0.021) for the greater stimulus, reflecting a greater capability of the larger stimulus in eliciting steal as predicted by the model.

Continuous distributions of CBF over a hypocapnic to hypercapnic range in the presence of regional autoregulatory compromise

All of the CVR maps from the patient cohort showed regions of steal. We analyzed these changes over the continuum of $P_{ET}CO_2$ from hypocapnia to hypercapnia. In a Supplementary video we show the dynamic changes in BOLD as a function of $P_{ET}CO_2$ in one patient. The video shows a cursor following the $P_{ET}CO_2$ stimulus on the left, and a 3D view of the BOLD MRI signal map response on the right. Fig. 5 shows a synopsis of the changes in BOLD MRI over 4 discreet intervals, illustrating the development of steal with all increases in $P_{ET}CO_2$ and reverse steal (Robin Hood effect) (Lassen and Palvolgyi, 1968) with all reductions in $P_{ET}CO_2$.

In this patient, reducing $P_{ET}CO_2$ from 40 mm Hg to 30 mm Hg produces a robust constriction in the healthy left brain territory and a decrease in the blood flow and BOLD signal (Fig. 5A). The CVR is color coded as before, but with the convention that its sign follows the BOLD change, so the CVR map is predominantly blue in the 'normal' vascular beds which vasoconstrict with reductions in $P_{ET}CO_2$. However, a careful inspection of map A shows some yellow and orange coloration in the right MCA territory, the side of the lesion, indicating areas where blood flow *increased* due to reverse steal, as predicted by the model (Fig. 2). With a further increase in $P_{ET}CO_2$ from 30 to 40 mm Hg there was a large increase in flow in the healthy left MCA region, but a lesser increase in the compromised right MCA region (Fig. 5B), indicating some residual vasodilatory reserve. Nevertheless, as predicted in Fig. 2, further hypercapnia to 50 mm Hg resulted in a greater stimulus to the healthy vessels, and in steal from the right middle cerebral artery (Fig. 5C). Finally, our conceptual model predicts that withdrawal of the vasodilatory stimulus will abolish the steal, allowing the restoration of rCBF, appearing as a positive change in flow (Fig. 5D).

Note that the pattern of red voxels in Fig. 5C is very similar to that of the dark blue voxels in Fig. 5D, indicating that these areas have a highly reactive vasculature with considerable reserves of vasodilation and vasoconstriction. However, the area which develops steal when $P_{ET}CO_2$ is increased from 40 mm Hg to 50 mm Hg (Fig. 5C blue, right brain) does not seem to undergo the same degree of change on the return of $P_{ET}CO_2$ to 40 mm Hg. We suggest the following explanation: During a generalized vasodilation, blood flow is drawn away from the tissues with low responsiveness by the robust vasodilation in high response tissues. However, the restoration of vasoconstriction in the high response tissues does not actually force blood back into the low response tissues, but rather simply reduces their blood flow demand, thereby allowing the low response tissues to re-establish their flow. A time dependence for this re-establishment of flow results in a hysteresis of the dynamic response to $P_{ET}CO_2$, which may account for the lesser degree of change when $P_{ET}CO_2$ returns to 40 mm Hg. With our present state of knowledge, it is only safe to say that this figure demonstrates that steal and reverse steal occur in the same territory and represent the same pathophysiological phenomenon, both in the hypocapnic and hypercapnic ranges, as predicted by the conceptual model (Fig. 2).

Changes in rCBF as a function of vasodilatory reserve

Fig. 6 presents examples of the BOLD signal as a function of a $P_{ET}CO_2$ ramp change taken from predominantly red, yellow and blue regions of interest for patient 5 (shown in Fig. 5). This process yields BOLD signal vs. $P_{ET}CO_2$ curves of the same shape as those demonstrated by Harper

Table 2
The characteristics of the whole brain population of voxel CVR values (%/mm Hg) for the patients and healthy volunteers at two $P_{ET}CO_2$ stimulus ranges, 40 to 45 mm Hg and 40 to 50 mm Hg using the ramp stimulus. *, §, †, # and ¶ pairs indicate statistical significance at P < 0.05.

Characteristic	Patients		Healthy volunteers	
	40–45 mm Hg	40–50 mm Hg	40–45 mm Hg	40-50 mm Hg
Mean	0.19 (0.16)	0.18 (0.1)	0.24 (0.14)	0.25 (0.07)
SD	1.02 (1.72)	0.64 (0.59)	1.26 (1.6)	0.85 (0.73)
Variance	3.8 (12.94)	0.74 (1.72)	3.98 (9.43)	1.21 (2.29)
Kurtosis	1446.37 (2358.81)	1289.42 (2892.99)	2644.27 (5068.31)	2481.66 (4466.52)
Median	0.11 (0.11)	0.11 (0.08)	0.17 (0.1)	0.17 (0.04)
Mode	19.57 (85.56)	14.58 (28.08)	27.76 (94.53)	18.15 (43.42)
Skewness	0.39 (32.38)	17.44 (27.98)	9.64 (44.81)	18.38 (34.44)
Mean + ve	0.37 (0.16)*	0.3 (0.1)*	0.42 (0.13)§	0.34 (0.08)§
Mean − ve	−0.22 (0.09)†	−0.16 (0.07)†	−0.25 (0.14)#	−0.16 (0.06)#
% − ve	31.33 (15.82)	28.84 (14.65)¶	24.13 (13.28)	17.5 (6.11)¶

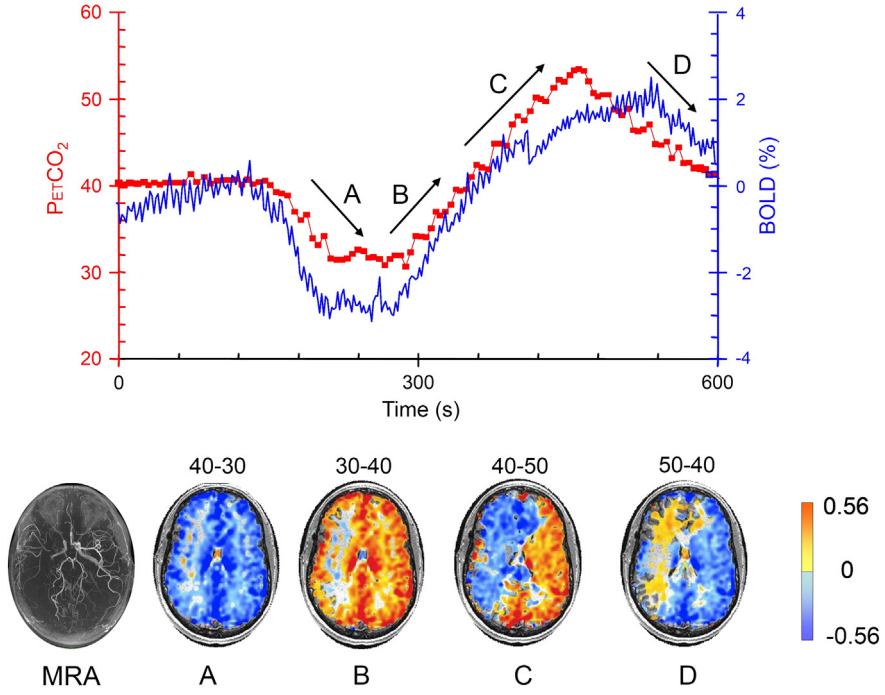

Fig. 5. CVR maps for an axial slice for different $P_{ET}CO_2$ changes in an 18 year old male with moyamoya disease affecting the right MCA territory (to the left of the figure) (MRA, on left). The top chart shows the $P_{ET}CO_2$ stimulus sequence (red) with the whole brain average BOLD signal changes (blue). Maps A to D represent changes in blood flow corresponding to changes in $P_{ET}CO_2$ as indicated by the arrows in the figure. Changes in blood flow are color coded according to the reference scale on the right of the CVR maps: orange and red represent interval increases in blood flow and blue represents interval reductions.

and Glass (1965) in dogs and Ringelstein et al. (1988) in humans (see Appendix A), and our conceptual model (Fig. 2).

Fig. 7A shows that the changes in the BOLD signal closely follow the changes in $P_{ET}CO_2$ in a voxel with presumably excellent vasodilatory reserve in one patient. The range of $P_{ET}CO_2$ appears to be substantially within the linear aspect of the curve. Fig. 7B shows the BOLD signal from a voxel that appears to simultaneously follow the $P_{ET}CO_2$ in an opposite pattern of flow from that in Fig. 7A. This response pattern is interpreted as due to the vasculature passively following the flow changes in the active regions because they are themselves unable to actively change their tone. Whereas Fig. 5 illustrates the model principle of redistribution of blood flow between territories, Fig. 7 illustrates the same principle in single voxels, in this case one with no vasodilatory reserve.

The same pattern is seen with a larger region of interest (ROI) with uniform response in the voxels. For the general case, where larger ROIs are chosen, the CVR will be an average of the range of BOLD responses represented in Fig. 6, including those that invariably overlap CSF and white matter resulting in a lower average gray matter CVR (Fig. 8).

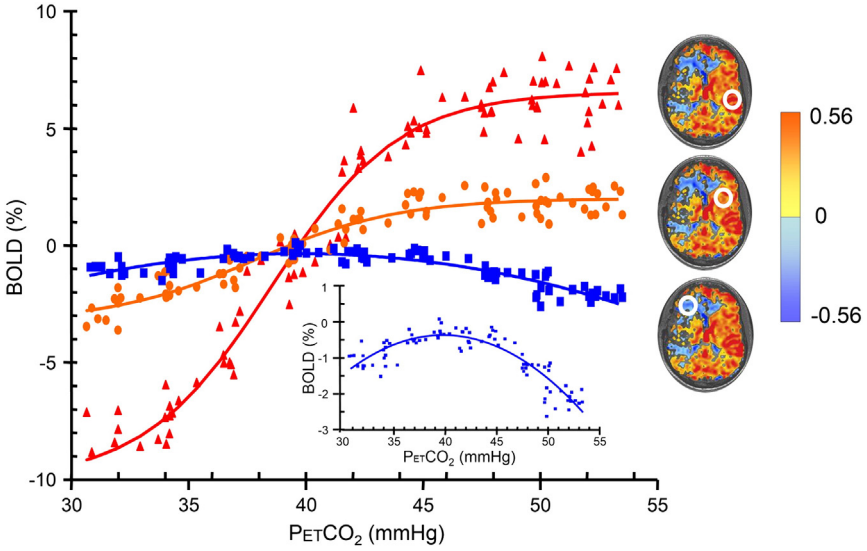

Fig. 6. Fitted BOLD responses to $P_{ET}CO_2$ in selected regions of interest (enclosed by the white circles) for patient 5 (shown in Fig. 5). A red region (top map) with a robust sigmoidal response (filled triangles and red line). A yellow region (middle map) with a moderate sigmoidal response (filled circles and orange line). A blue region (bottom map) with a poor response showing steal (squares and blue line). The inset (lower right) shows the latter response with an expanded BOLD scale to show the curvature in this response.

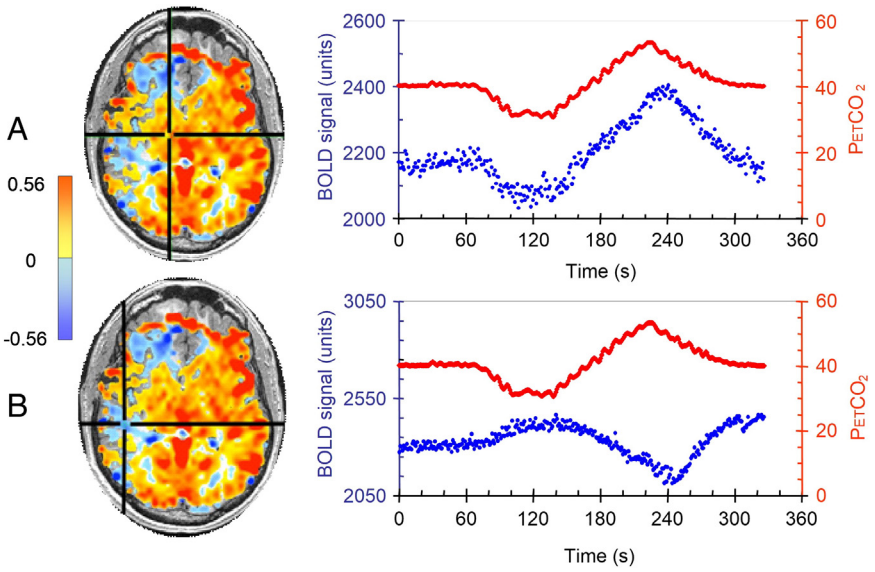

Fig. 7. Voxel tracking of $P_{ET}CO_2$. CVR maps are shown on the left with chosen voxels indicated by the cross hairs. The right side shows graphs of the chosen voxels BOLD signals (blue dots) in response to the changes in $P_{ET}CO_2$ (red dots). In each case the BOLD signals track the $P_{ET}CO_2$ stimulus, indicating that precise and accurate measurement of CVR requires accuracy and precision of the $PaCO_2$ stimulus as well as the surrogate measure of CBF (reproduced from Fierstra et al., 2013).

Discussion

Main findings

The main finding of this study is that a model of the distribution of CBF in response to hypercapnia described in 1968, enhanced by incorporating subsequently published observations, was successful in accounting for the pattern of CVR observed in healthy subjects, as well as in patients with a range of extracranial and intracranial steno-occlusive vascular disease. Overall, the data was consistent with the following aspects of the model. The observed smaller CVR values with the greater hypercapnic provocation in areas with positive CVR are the result of a sigmoid relationship between the $PaCO_2$ and CBF in each isolated vascular region. The identification of reversing vascular response curves, where rCBF increases with small increases in $P_{ET}CO_2$, and then reverses this relationship with higher $P_{ET}CO_2$ (Fig. 6), confirms the predictions shown in Fig. 2.

The observation of reciprocal flow responses in territories with changes in stimulation direction (Figs. 5 and 7) suggests that the two flows are co-dependent, and therefore compete for the same total flow; otherwise their changes in flow would be in the same direction. The dependence of the reduction in flow in the compromised territory on the increase in flow in other territories is also supported by their simultaneous occurrence, despite delayed circulation (and arrival of a change in $PaCO_2$) to the compromised territory (Poublanc et al., 2013). The extent of redistribution reflects the balance between the magnitude of the stimulus and the relative vasodilatory capacity of vascular regions perfused in parallel. The reduction in the range of positive and negative CVR values with the greater provocation is explained by reference to Fig. 4 and its associated text. The model may also help

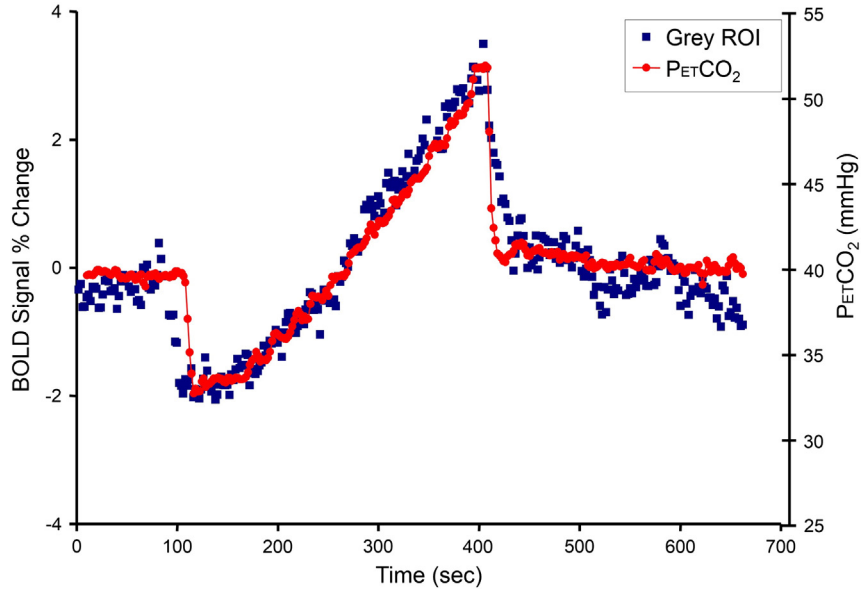

Fig. 8. The average BOLD signal in a gray matter region of interest (ROI) during a ramp test protocol. Note that there is a continuous proportional change of % BOLD with $P_{ET}CO_2$.

in choosing the baseline level, and range of $P_{ET}CO_2$ change to optimize the interpretation of CVR, or retrospectively, to identify limitation in its interpretation (illustrated in Fig. 5).

CVR and pathophysiology

This work provides some insights into the interpretation of CVR, particularly its limitations. CVR values are not a linear function of the strength of the stimulus. Rather, they are related in a complex way, not only as a result of the sigmoidal relationship between stimulus and vasodilation, but also the superimposition of conditions resulting in the redistribution of flow between vascular territories. It is noteworthy that, as we have shown, small stimuli result in greater CVR values, but larger stimuli are more sensitive for identifying reductions of vasodilatory reserve. Without a sufficiently large stimulus, the global CBF demand may not exceed the supply capacity, and redistribution between large vascular territories may not be apparent; however more peripheral flow limitations may be exposed by downstream redistributions of flow with less stimulation. In many published works, great care was not taken in specifying—or even accurately measuring—the magnitude of the stimulus (Fierstra et al., 2013). As our experiments and the model show, knowing the baseline and amplitude of the stimulus is indispensable to CVR interpretation. We have also noted that the same may be true of other parameters such as the time course of the test and the sequence of $P_{ET}CO_2$ changes.

Finally we note that whereas the demonstration of steal is indicative of underlying pathology, its absence may be more difficult to interpret (Persoon et al., 2012). CVR requires a differential effect of the vasodilator on vascular territories, which may be absent if blood vessels throughout the brain respond uniformly—even if this response is abnormal. Thus, according to our model, there would be no steal in the presence of diffuse pathology, as may occur, for example, in Alzheimer's dementia, vasculitis or brain blast injury. There would also not be any steal in a vascular bed with a relatively independent perfusion (i.e., not co-dependent with another territory for a limited blood supply).

The relationship between CVR and the blood flow at rest

Our model is consistent with the recently proposed classifications of cerebrovascular reserve. Derdeyn et al. (2002) defined Stage I loss of vascular reserve as that where autoregulatory vasodilation is the predominant response to a progressive reduction in perfusion pressure; where the CBF lags behind in meeting brain oxygen demand the shortfall is met by small increases in oxygen extraction fraction (OEF). In Stage II, increases in OEF are insufficient to meet the brain metabolic demand (as measured by P_{ET}). Kuroda et al. (1993) described three patterns of CBF (as measured by 133-Xe SPECT) at rest and in response to a vasodilatory stimulus (acetazolamide). Type 1 and Type 2 have normal blood flow at rest, and normal and reduced CVR respectively. Type 3 has both reduced CBF and CVR. For comparison of these models to ours with BOLD CVR we present 2 example cases from our patient cohort where, in addition to CVR, resting CBF was measured by arterial spin labeling (ASL) prior to CVR measures. Fig. 9A (subject 1) presents a patient with normal resting CBF and reduced CVR. This patient would be classed as Powers Stage I (OEF likely normal) and Kuroda Type 2. Fig. 9B presents a patient with reduced resting blood flow on the left and reduced CVR. This patient would be classed Powers Stage II and Kuroda Type 3. Of note, Fig. 9A emphasizes the added diagnostic value of a provocative stimulus, in this case CVR, above resting CBF or OEF.

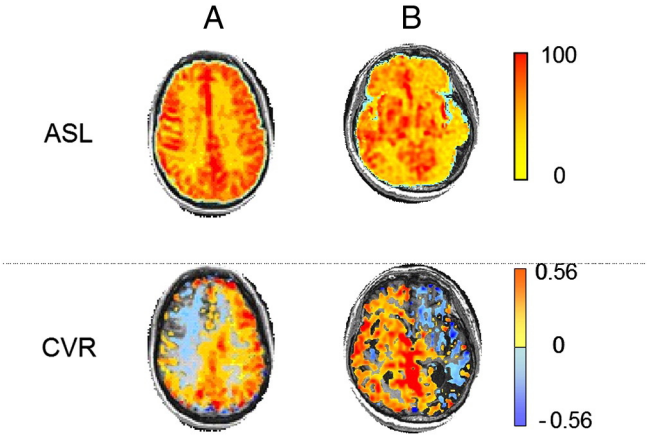

Fig. 9. Comparison of resting blood flow measured by ASL, and CVR. (A) An asymptomatic 18 year old female (Subject 1) with moyamoya disease and previous right extracranial–intracranial bypass; right hemispheric blood flow appears normal but CVR is reduced. (B) a 75 year old male with intracranial atherosclerosis and LICA occlusion; both ASL and CVR are reduced. ASL and CVR units are mL/min/100 g and Δ%BOLD MR signal/ΔmmHg$P_{ET}CO_2$, respectively.

Advantages of our CVR data for examining the model

Our experimental data have a number of advantages for examining a CVR model. First, they were obtained from awake, non-sedated humans, including some with cerebrovascular disease; thereby addressing the issue of applicability of the model to clinical conditions. Second, the CVR calculations benefitted from the high time (2 s) and spatial (3.75 × 3.75 × 5 mm voxels) resolution of the BOLD signals, and the accuracy and the breath-by-breath time resolution of the stimulus ($PaCO_2$), so that it was possible to generate a dataset of pseudo-continuous CVR values over a large range of $PaCO_2$ (from hypo- to hypercapnia). Observing the changes in CVR over such a continuum of $PaCO_2$ provides insight into the sequences of the changes that occur when only a single stimulus is administered, such as breath-hold, inhaled carbogen, and injection of acetazolamide.

As a final note, we point out that the $P_{ET}CO_2$ stimuli in this study were implemented in a highly controlled and predictable manner using a custom gas blender and sequential gas delivery system described by Slessarev et al. (2007). However, similar patterns of stimulation can be implemented by end-tidal forcing (Beaudin et al., 2011) coached hyperventilation coupled with rebreathing (Battisti-Charbonney et al., 2011) or supplementation of inhaled gas with CO_2 (Ringelstein et al., 1992) as reviewed in Fierstra et al. (2013).

Limitations

Sex difference in healthy and patient cohorts

The predominance of females (13/16) in the patient cohort reflects the greater incidence of moyamoya in females, i.e., 2:1 (Scott and Smith, 2009). Indeed, a count of the first 50 charts retrieved from our hospital records with a diagnosis of moyamoya yielded only 3 male names. In the healthy cohort the predominance of males represents the results of an unselective recruitment process. However, our most important observations are related to the redistribution of blood flow, which are within-subject changes independent of differences in cohorts. An exception is our observation of a greater fraction of voxels with negative CVR at the larger stimulus in the patient cohort. We report this finding as consistent with the predictions of our model, but cannot rule out sex as a factor.

Insensitivity of statistical methods to discriminate between groups

The lack of a significant difference in the kurtosis and skewness parameters of the CVR distributions between the healthy cohort and patients was somewhat surprising in that the distributions

appear to be different in these respects by eye. These parameters therefore lack sufficient sensitivity to be used clinically. We suggest that the explanation lies in the combination of the large number of voxels in the analysis for each subject, the small range of CVR values in the positive and negative ranges, and the considerable overlap of pathological and normal CVR values. Discrimination may be improved by taking into account other dimensions of these measurements, such as the spatial distribution of CVR and the time course of the BOLD signal change. However, in this paper we focus on a conceptual model delineating the mechanism of steal in an effort to inform the quest for methods of optimizing the sensitivity and specificity for identification of pathological neurovascular conditions.

BOLD as a surrogate for CBF

Tancredi and Hoge (2013) showed that, in the $P_{ET}CO_2$ range of 40 to 50 mm Hg, CBF measured by arterial spin labeling (ASL) is a linear function of $P_{ET}CO_2$. While ASL measurements are incompatible with our ramp stimulus protocol, we nevertheless must consider that the BOLD signal is affected by the cerebral metabolic rate of O_2 consumption ($CMRO_2$), change in blood volume, and by signal drift. Although we corrected for signal drift, a potential nonlinearity effect remains if there are changes in $CMRO_2$ and cerebral blood volume (CBV). In addition, small negative changes in BOLD can occur in specific voxels bordering CSF that are not coupled to flow, but rather to changes in brain volume (Bright et al., 2014; Thomas et al., 2013). It is well known that the BOLD signal is not just dependent on blood flow. The scale of the blood flow is dependent on the resting deoxyhemoglobin level and changes in concentration, as well on the oxygen extraction. Nevertheless, we repeatedly observed that the BOLD signal seemed to follow that of expected blood flow in pathological as well as normal regions in our patients. Figs. 5 and 7 illustrate this by showing the repeated reciprocal changes of BOLD signal in pathological and healthy areas of the brain, consistent with the corresponding changes in blood flow predicted by our model. Furthermore, the timing of the changes in the pathological areas, rather than being delayed or dampened, is brisk and simultaneous with those in the healthy areas (Poublanc et al., 2013), also indicating that they are due to redistribution of blood flow passively following the changes in the briskly reacting vascular beds. The close tracking of the BOLD signal in both the healthy and pathological areas with PCO_2 indicates that any nonlinear relationship between BOLD signal and CBF must be small compared to the effect of PCO_2 on CBF itself.

Conclusion

The CVR maps in patients with known cerebral vascular pathology were consistent with the predictions of an enhanced version of a 1968 model to explain cerebral steal. This enhanced model may now, in turn, be invoked to provide a hemodynamic interpretation to CVR maps.

Supplementary data to this article can be found online at http://dx.doi.org/10.1016/j.neuroimage.2014.01.051.

Acknowledgments

We are grateful to the Toronto Western Hospital MRI technologists, in particular Eugen Hlasny and Keith Ta for the help in acquiring the data and to Steve Iscoe for the editing assistance.

Disclosure/declaration of interest

JAF is the Chief Scientist and JD is a Senior Scientist at Thornhill Research Inc. (TRI), a spin-off company from the University Health Network that developed the RespirAct™. RespirAct™ is currently a non-commercial research tool assembled by TRI to enable CVR studies.

Appendix A

Background cerebrovascular physiology

The perfusion pressure for any regional vascular territory of the brain is the systemic blood pressure minus any reductions in pressure due to flow resistance in the major vessels arising from the Circle of Willis (assuming venous backpressure and intracranial pressure are not limiting). The latter flow resistances may be variable, due to changes in vascular tone, or fixed, due to steno-occlusive lesions. Autoregulation reduces the downstream vascular tone in an attempt to match flow to the metabolic requirements of the perfused tissues (Hill et al., 2006; Lucas et al., 2010). However, such a decrease in vascular tone has a physical limit, and the difference between this limit and the resting vessel tone constitutes a *vascular vasodilatory reserve*.[1] Autoregulation can maintain normal resting flow despite as much as 70% blockage of the upstream feed vessel. However, when a generalized vasodilatory stimulus is applied, the blood flow to the post-stenotic vascular bed is challenged, often resulting in a paradoxical *reduction* in flow (steal) (Brawley, 1968; Mandell et al., 2008). The three conditions required for steal to occur are (a) two or more intra-cranial vascular beds with different vasodilator reserve capacities; (b) the vascular beds are perfused in parallel from a common arterial blood supply; and (c) the flow capacity of this supply is less than that of the vascular beds.

In healthy brain, most (but not all; Mandell et al., 2008) vascular beds will increase their flows, and any effects of the limitation of inflow may not be apparent. However, the major extracranial vessels provide at least 30% of the total resistance to flow—much more than similarly sized vessels elsewhere in the body (Faraci and Heistad, 1990). The increase in flow induced by a strong vasodilatory stimulus may exceed the supply capacity resulting in a reduction in pial perfusion pressures (Brawley, 1968) and establishing conditions for a competition for perfusion *between* intracranial vascular territories perfused in parallel (Symon, 1968).

In this section, we draw on previously published data to further develop the concepts of redistribution of cerebral blood flow (CBF) and extend this model to cover a wide range of autoregulatory encroachments in disparate vascular beds, strengths of vasodilatory stimuli, and baseline conditions.

Harper and Glass (1965) examined the CBF response to CO_2 as a function of perfusion pressure in dogs. As perfusion pressure was reduced from normal, the change in CBF in response to a given change in PCO_2 was less (Figs. 1A, B). Indeed, below a threshold perfusion pressure, CBF was unresponsive to PCO_2 (Fig. 1C). At this lowest pressure, autoregulatory-mediated vasodilation was maximal. Vessels could neither vasodilate further in response to hypercapnia, nor overcome autoregulation and constrict in response to hypocapnia (Brawley, 1968). We re-analyzed these data to illustrate the relationship between autoregulatory reserve, and responses to changes in PCO_2. First, we re-scaled all three responses presented in the original figures from Harper and Glass (1965), and plotted them on the same graph (Fig. 1D). This rearrangement shows that the vascular tone at resting $PaCO_2$ is in the mid-range, retaining some degree of constrictor and dilator reserve. Second, assuming that at maximal $PaCO_2$, the resistance vessels are all maximally dilated regardless of their perfusion pressures (Symon, 1969), we re-plotted the data as 'percent maximal dilation' vs. $PaCO_2$ (Fig. 1E).

[1] We develop the model on the basis of regional vascular stenosis where "autoregulatory reserve" is appropriate. However, we prefer 'vasodilatory reserve' as it is more general as it can also be applied to vessels that are plegic due to, for example, drugs, developmental vascular abnormalities, vascular disease, or trauma.

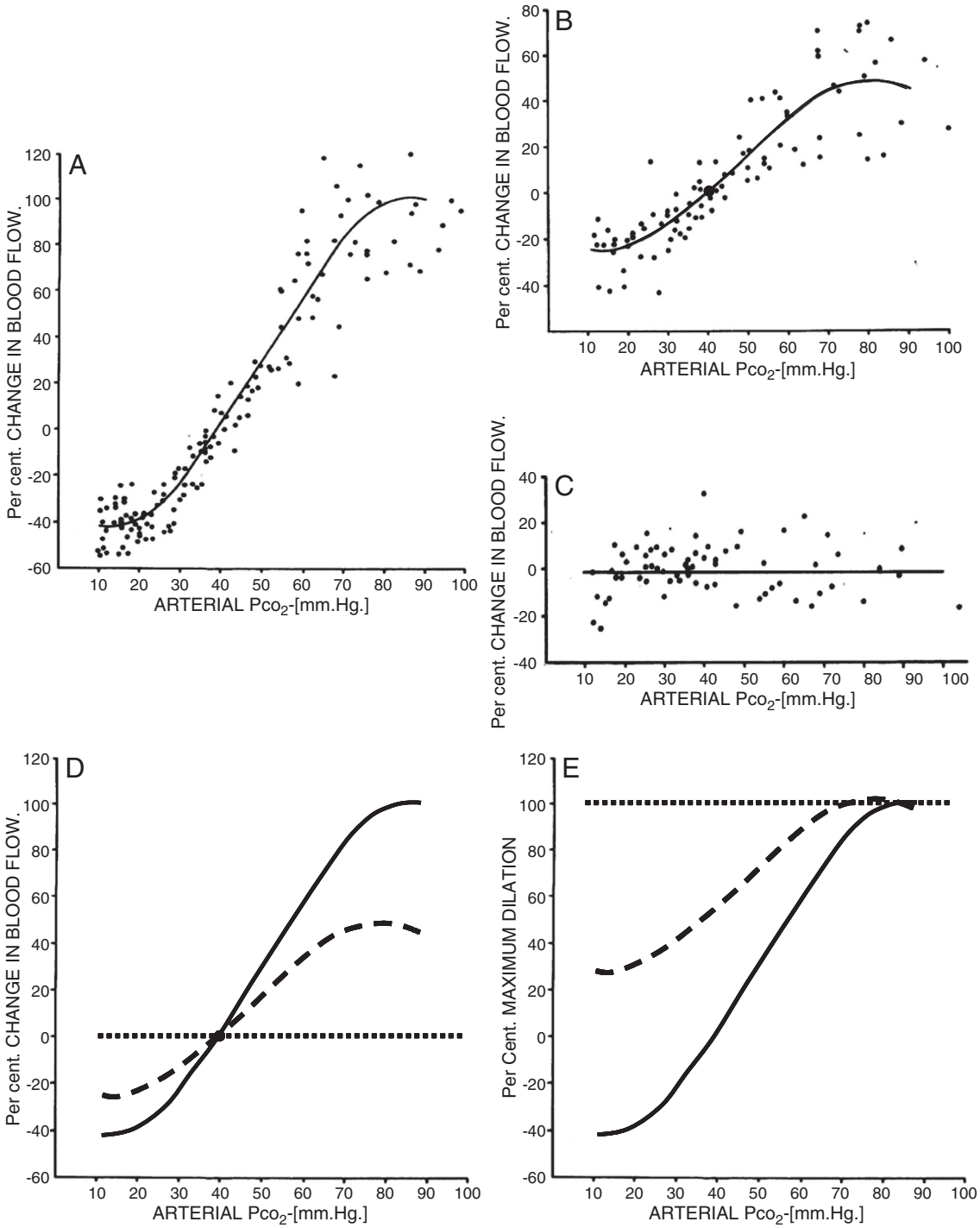

Appendix A. Fig. 1. Results redrawn from experiments in dogs by Harper and Glass (1965; Figs. A, B, and C) showing the effects of reducing perfusion pressure on the CBF response to CO_2. A) Normotensive; B) Hypotensive; C) Extreme hypotension; D) An overlay of the fitted responses in A and B drawn to the same scale; E) The fitted responses presented as the % of maximum vasodilation.

The analysis of these data allows the extension of the original 'cerebral steal' description to include the following enhancements. First, the relationship between $PaCO_2$ and CBF is sigmoidal. Second, encroachment on the vasodilatory reserve by autoregulatory-induced vasodilation reduces the reactivity to CO_2, as indicated by a reduction in the slope of the linear part of the sigmoid. Third, when autoregulation is exhausted, there is no further response to hypercapnia. Fourth, the midpoint of the sigmoid curve is approximately at the resting PCO_2. Finally, we note that hypocapnia incompletely reverses autoregulatory vasodilation.

Next, we examined whether these relations observed in the dogs of Harper and Glass (1965) occur in humans. Ringelstein et al. (1988) examined patients with unilateral carotid artery stenosis, a condition where compromised and uncompromised regions of the brain can be identified, and where both regions are perfused in parallel by common feed vessels. Fig. 2 is modified from their data and graphs. We graphed the changes in blood flow as a function of $PaCO_2$ in patients with various encroachments on their autoregulatory reserve, on the same axes as in Fig. 1D. The reduced vascular response to changes in PCO_2 in the presence of an upstream stenosis (Fig. 2C) compared to the response of the normal side (Fig. 2A) is similar to that observed by Harper and Glass (1965) in the whole brain.

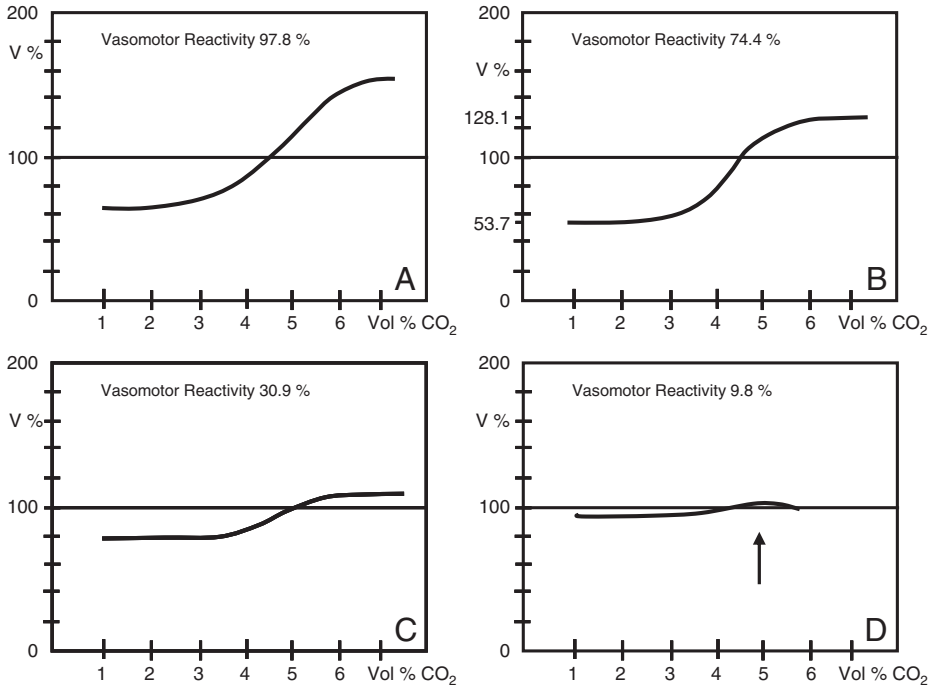

Appendix A. Fig. 2. An illustration of the effects of CO_2 on CBF (Figs. 1, 2 & 3) redrawn from Ringelstein et al. (1988) from experiments in humans with varying degrees of unilateral carotid stenosis. Resting PCO_2 values correspond to the horizontal lines. The abscissa is end tidal fractional concentration of CO_2 expressed as percent. The ordinate scale represents percent of normal values (100%) A) The line of best fit through a series of responses in a sample of 40 healthy individuals, ages 20 to 75. B) A near normal response on the non-occluded side of a patient; and C) a reduced response on the occluded side; D) A near absent response on the occluded side in a patient with a carotid artery occlusion. Note the reduction of velocity at a high PCO_2 (arrow). (V% = middle cerebral artery blood velocity; vasomotor reactivity was calculated as total change in velocity as percent of normocapnic values.).

A conceptual model

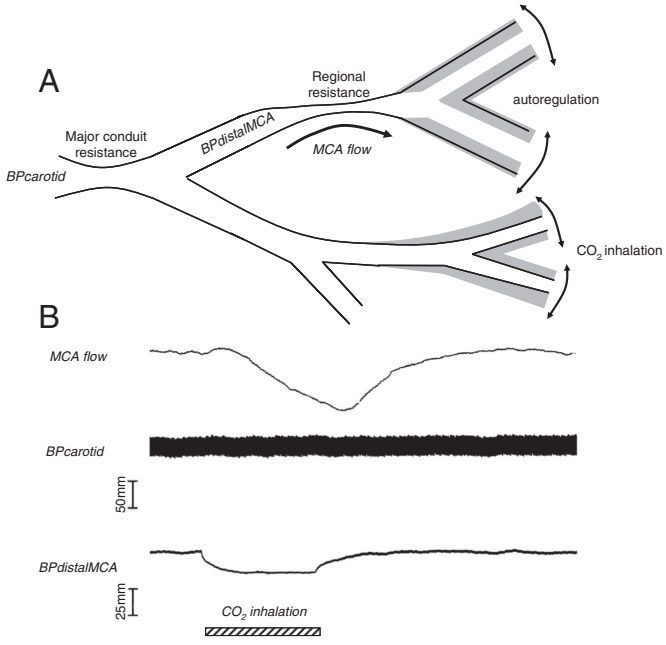

Appendix A. Fig. 3. Upper panel, schematic illustration of the vascular model showing resistance in extra-cranial supply vessels and a stenotic lesion in an intracranial vessel such as the middle cerebral artery (MCA). Lower panel is data from this model examined in a dog (figure modified from Brawley, 1967) with pressure measured in the carotid artery (BPcarotid) and distal MCA (BPdistalMCA) and flow measured in the distal MCA. The hypercapnic stimulus is designated by the hatched line. This data is interpreted as distal vasodilation in healthy vascular beds reducing the perfusion pressure of the MCA resulting in a reduction blood flow.

Fig. 3 summarizes the model. At rest, vessels perfused via the stenosed branch are dilated to supply their tissues' metabolic requirements, and blood flow may appear normal. However, with a progressively increasing vasodilatory stimulus, the dilation may reach its limit, and blood flow may decline as the limited blood supply is diverted to the vessel with dilatory reserve (Fig. 3B).

This scenario can be applied to predict the regional cerebral blood flow (rCBF) response to a range of changes in $PaCO_2$ as shown in Fig. 4. Note that Fig. 4 illustrates the response to CO_2 in a branch with reduced vasodilatory reserve when stimulated in isolation (dashed line) and during a global stimulus (dotted line). The vessel with the reduced reserve may not increase its flow, or may even reduce its flow in response to the global hypercapnic stimulus, depending on the magnitude of the stimulus, the vasodilatory reserve of the vessels in the stenosed branch as well as the extent of the response of the vessels in the normal branch.

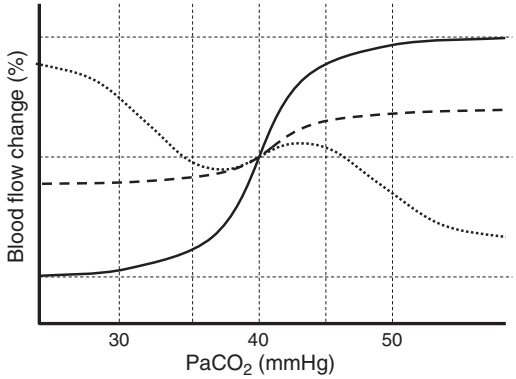

Appendix A. Fig. 4. The responses to $PaCO_2$ predicted for the model of a brain vascular territory with a partially-stenosed vessel branch and a healthy branch in parallel. The solid line depicts the sigmoidal CBF response of a normal vessel in isolation. The dashed line depicts the flow in a vessel with reduced autoregulatory reserve. The dotted line depicts the response of the same compromised vessel when perfused in parallel with the normal vessel branch under conditions where flow to the complex is limiting. Note the prediction of steal with hypercapnia and reverse steal with hypocapnia.

Summary

This model was developed from the early concepts of steal by incorporating the experimental results obtained in the ensuing years to produce the dynamic model we propose here, which has the following defining characteristics:

(a) The relation between flow and vasodilatory stimulus for each vascular territory is sigmoidal when stimulated in isolation, with a midpoint close to resting $PaCO_2$.
(b) Each vascular territory therefore has a vasodilatory reserve, which autoregulation may draw upon to ensure an adequate blood flow.
(c) Vascular territories perfused in parallel from a single source compete for flow during a global stimulus because the source flow is limited.

As a result of these characteristics, vascular territories may be able to maintain an adequate blood flow under resting conditions by encroaching on their vasodilatory reserve, and even respond to moderate metabolic demands. However, when stressed by an increased demand or a global vasodilatory stimulus such territories are unable to compete for the limited flow supply and have their flow stolen by their neighbors with excess vasodilatory reserve. Thus, to identify such vascular territories an adequate global stimulus is needed.

References

Battisti-Charbonney, A., Fisher, J., Duffin, J., 2011. The cerebrovascular response to carbon dioxide in humans. J. Physiol. 589, 3039–3048.

Beaudin, A.E., Brugniaux, J.V., Vohringer, M., Flewitt, J., Green, J.D., Friedrich, M.G., Poulin, M.J., 2011. Cerebral and myocardial blood flow responses to hypercapnia and hypoxia in humans. Am. J. Physiol. Heart Circ. Physiol. 301, H1678–H1686.

Brawley, B.W., 1968. The pathophysiology of intracerebral steal following carbon dioxide inhalation, an experimental study. Scand. J. Clin. Lab. Invest. Suppl. 102 (XIII:B).

Bright, M.G., Bianciardi, M., de Zwart, J.A., Murphy, K., Duyn, J.H., 2014. Early anti-correlated BOLD signal changes of physiologic origin. NeuroImage 87, 287–296.

Brogan, T.V., Robertson, H.T., Lamm, W.J., Souders, J.E., Swenson, E.R., 2004. Carbon dioxide added late in inspiration reduces ventilation–perfusion heterogeneity without causing respiratory acidosis. J. Appl. Physiol. 96, 1894–1898.

Cox, R.W., 1996. AFNI: software for analysis and visualization of functional magnetic resonance neuroimages. Comput. Biomed. Res. 29, 162–173.

Derdeyn, C.P., Videen, T.O., Yundt, K.D., Fritsch, S.M., Carpenter, D.A., Grubb, R.L., Powers, W.J., 2002. Variability of cerebral blood volume and oxygen extraction: stages of cerebral haemodynamic impairment revisited. Brain 125, 595–607.

Faraci, F., Heistad, D., 1990. Regulation of large cerebral arteries and cerebral microvascular pressure. Circ. Res. 66, 8–17.

Fierstra, J., Poublanc, J., Han, J.S., Silver, F., Tymianski, M., Crawley, A.P., Fisher, J.A., Mikulis, D.J., 2010. Steal physiology is spatially associated with cortical thinning. J. Neurol. Neurosurg. Psychiatry 81, 290–293.

Fierstra, J., Machina, M., Battisti-Charbonney, A., Duffin, J., Fisher, J.A., Minkovich, L., 2011. End-inspiratory rebreathing reduces the end-tidal to arterial PCO(2) gradient in mechanically ventilated pigs. Intensive Care Med. 37, 1543–1550.

Fierstra, J., Sobczyk, O., Battisti-Charbonney, A., Mandell, D.M., Poublanc, J., Crawley, A.P., Mikulis, D.J., Duffin, J., Fisher, J.A., 2013. Measuring cerebrovascular reactivity: what stimulus to use? J. Physiol. 591, 5809–5821.

Harper, A.M., Glass, H.I., 1965. Effect of alterations in the arterial carbon dioxide tension on the blood flow through the cerebral cortex at normal and low arterial blood pressures. J. Neurol. Neurosurg. Psychiatry 28, 449–452.

Hill, M.A., Davis, M.J., Meininger, G.A., Potocnik, S.J., Murphy, T.V., 2006. Arteriolar myogenic signalling mechanisms: implications for local vascular function. Clin. Hemorheol. Microcirc. 34, 67–79.

Iadecola, C., Nedergaard, M., 2007. Glial regulation of the cerebral microvasculature. Nat. Neurosci. 10, 1369–1376.

Ito, S., Mardimae, A., Han, J., Duffin, J., Wells, G., Fedorko, L., Minkovich, L., Katznelson, R., Meineri, M., Arenovich, T., Kessler, C., Fisher, J.A., 2008. Non-invasive prospective targeting of arterial PCO_2 in subjects at rest. J. Physiol. 586, 3675–3682.

Kleiser, B., Widder, B., 1992. Course of carotid artery occlusions with impaired cerebrovascular reactivity. Stroke 23, 171–174.

Kuroda, S., Kamiyama, H., Abe, H., Houkin, K., Isobe, M., Mitsumori, K., 1993. Acetazolamide test in detecting reduced cerebral perfusion reserve and predicting long-term prognosis in patients with internal carotid artery occlusion. Neurosurgery 32, 912–918.

Lassen, N.A., Palvolgyi, R., 1968. Cerebral steal during hypercapnia and the inverse reaction during hypocapnia observed by the 133 xenon technique in man. Scand. J. Clin. Lab. Invest. Suppl. 102 (XIII:D).

Lucas, S.J., Tzeng, Y.C., Galvin, S.D., Thomas, K.N., Ogoh, S., Ainslie, P.N., 2010. Influence of changes in blood pressure on cerebral perfusion and oxygenation. Hypertension 55, 698–705.

Mandell, D.M., Han, J.S., Poublanc, J., Crawley, A.P., Stainsby, J.A., Fisher, J.A., Mikulis, D.J., 2008. Mapping cerebrovascular reactivity using blood oxygen level-dependent MRI in patients with arterial steno-occlusive disease: comparison with arterial spin labeling MRI. Stroke 39, 2021–2028.

Markus, H., Cullinane, M., 2001. Severely impaired cerebrovascular reactivity predicts stroke and TIA risk in patients with carotid artery stenosis and occlusion. Brain 124, 457–467.

Marshall, R.S., Lazar, R.M., 2011. Pumps, aqueducts, and drought management: vascular physiology in vascular cognitive impairment. Stroke 42, 221–226.

Molina, C., Sabin, J.A., Montaner, J., Rovira, A., Abilleira, S., Codina, A., 1999. Impaired cerebrovascular reactivity as a risk marker for first-ever lacunar infarction: a case–control study. Stroke 30, 2296–2301.

Ogasawara, K., Ogawa, A., Yoshimoto, T., 2002. Cerebrovascular reactivity to acetazolamide and outcome in patients with symptomatic internal carotid or middle cerebral artery occlusion: a xenon-133 single-photon emission computed tomography study. Stroke 33, 1857–1862.

Persoon, S., Kappelle, L.J., van Berckel, B.N., Boellaard, R., Ferrier, C.H., Lammertsma, A.A., Klijn, C.J., 2012. Comparison of oxygen-15 PET and transcranial Doppler CO_2-reactivity measurements in identifying haemodynamic compromise in patients with symptomatic occlusion of the internal carotid artery. EJNMMI Res. 2, 30.

Poublanc, J., Han, J.S., Mandell, D.M., Conklin, J., Stainsby, J.A., Fisher, J.A., Mikulis, D.J., Crawley, A.P., 2013. Vascular steal explains early paradoxical blood oxygen level-dependent cerebrovascular response in brain regions with delayed arterial transit times. Cerebrovasc. Dis. Extra 3, 55–64.

Ringelstein, E.B., Sievers, C., Ecker, S., Schneider, P.A., Otis, S.M., 1988. Noninvasive assessment of CO_2-induced cerebral vasomotor response in normal individuals and patients with internal carotid artery occlusions. Stroke 19, 963–969.

Ringelstein, E.B., Van Eyck, S., Mertens, I., 1992. Evaluation of cerebral vasomotor reactivity by various vasodilating stimuli: comparison of CO_2 to acetazolamide. J. Cereb. Blood Flow Metab. 12, 162–168.

Saad, Z.S., Glen, D.R., Chen, G., Beauchamp, M.S., Desai, R., Cox, R.W., 2009. A new method for improving functional-to-structural MRI alignment using local Pearson correlation. NeuroImage 44, 839–848.

Sasoh, M., Ogasawara, K., Kuroda, K., Okuguchi, T., Terasaki, K., Yamadate, K., Ogawa, A., 2003. Effects of EC–IC bypass surgery on cognitive impairment in patients with hemodynamic cerebral ischemia. Surg. Neurol. 59, 455–460.

Scott, R.M., Smith, E.R., 2009. Moyamoya disease and moyamoya syndrome. N. Engl. J. Med. 360, 1226–1237.

Silvestrini, M., Viticchi, G., Falsetti, L., Balucani, C., Vernieri, F., Cerqua, R., Luzzi, S., Bartolini, M., Provinciali, L., 2011. The role of carotid atherosclerosis in Alzheimer's disease progression. J. Alzheimers Dis. 25, 719–726.

Slessarev, M., Han, J., Mardimae, A., Prisman, E., Preiss, D., Volgyesi, G., Ansel, C., Duffin, J., Fisher, J.A., 2007. Prospective targeting and control of end-tidal CO_2 and O_2 concentrations. J. Physiol. 581, 1207–1219.

Spano, V.R., Mandell, D.M., Poublanc, J., Sam, K., Battisti-Charbonney, A., Pucci, O., Han, J.S., Crawley, A.P., Fisher, J.A., Mikulis, D.J., 2013. CO2 blood oxygen level-dependent MR mapping of cerebrovascular reserve in a clinical population: safety, tolerability, and technical feasibility. Radiology 266, 592–598.

Symon, L., 1968. Experimental evidence for "intracerebral steal" following CO_2 inhalation. Scand. J. Clin. Lab. Invest. Suppl. 102 (XIII:A).

Symon, L., 1969. The concept of intracerebral steal. Int. Anesthesiol. Clin. 7, 597–615.

Tancredi, F.B., Hoge, R.D., 2013. Comparison of cerebral vascular reactivity measures obtained using breath-holding and CO2 inhalation. J. Cereb. Blood Flow Metab. 33, 1066–1074.

Thomas, B.P., Liu, P., Aslan, S., King, K.S., van Osch, M.J., Lu, H., 2013. Physiologic underpinnings of negative BOLD cerebrovascular reactivity in brain ventricles. NeuroImage 83, 505–512.

Webster, M.W., Makaroun, M.S., Steed, D.L., Smith, H.A., Johnson, D.W., Yonas, H., 1995. Compromised cerebral blood flow reactivity is a predictor of stroke in patients with symptomatic carotid artery occlusive disease. J. Vasc. Surg. 21, 338–344.

Willie, C.K., Ainslie, P.N., 2011. Cool head, hot brain: cerebral blood flow distribution during exercise. J. Physiol. 589, 2657–2658.

Yonas, H., Smith, H.A., Durham, S.R., Pentheny, S.L., Johnson, D.W., 1993. Increased stroke risk predicted by compromised cerebral blood flow reactivity. J. Neurosurg. 79, 483–489.

Zhao, P., Alsop, D.C., Abduljalil, A., Selim, M., Lipsitz, L., Novak, P., Caplan, L., Hu, K., Novak, V., 2009. Vasoreactivity and peri-infarct hyperintensities in stroke. Neurology 72, 643–649.